International Journal of
Molecular Sciences

MDPI

Article

Synthesis and Structural Optimization of 2,7,9-Trisubstituted purin-8-ones as FLT3-ITD Inhibitors

Monika Tomanová [1,†], Karolína Kozlanská [2,†], Radek Jorda [2], Lukáš Jedinák [1], Tereza Havlíková [1], Eva Řezníčková [2], Miroslav Peřina [2], Pavel Klener [3,4], Alexandra Dolníková [3], Petr Cankař [1,*] and Vladimír Kryštof [2,5,*]

1 Department of Organic Chemistry, Faculty of Science, Palacký University Olomouc, 17. listopadu 1192/12, 77900 Olomouc, Czech Republic
2 Department of Experimental Biology, Faculty of Science, Palacký University Olomouc, Šlechtitelů 27, 78371 Olomouc, Czech Republic
3 First Faculty of Medicine, Institute of Pathological Physiology, Charles University, 12108 Prague, Czech Republic
4 First Department of Internal Medicine-Hematology, General University Hospital and First Faculty of Medicine, Charles University, 12808 Prague, Czech Republic
5 Institute of Molecular and Translational Medicine, Faculty of Medicine and Dentistry, Palacký University Olomouc, Hněvotínská 5, 77900 Olomouc, Czech Republic
* Correspondence: petr.cankar@upol.cz (P.C.); vladimir.krystof@upol.cz (V.K.)
† These authors contributed equally to this work.

Abstract: Therapy of FLT3-positive acute myeloid leukemia still remains complicated, despite the availability of newly approved kinase inhibitors. Various strategies to avoid the reduced efficacy of therapy have been explored, including the development of dual targeting compounds, which inhibit FLT3 and another kinase necessary for the survival and proliferation of AML cells. We have designed new 2,7,9-trisubstituted 8-oxopurines as FLT3 inhibitors and report here the structure-activity relationship studies. We demonstrated that substituents at positions 7 and 9 modulate activity between CDK4 and FLT3 kinase, and the isopropyl group at position 7 substantially increased the selectivity toward FLT3 kinase, which led to the discovery of compound **15a** (9-cyclopentyl-7-isopropyl-2-((4-(piperazin-1-yl)phenyl)amino)-7,9-dihydro-8*H*-purin-8-one). Cellular analyses in MV4-11 cells revealed inhibition of autophosphorylation of FLT3 kinase in nanomolar doses, including the suppression of downstream STAT5 and ERK1/2 phosphorylation. We also describe mechanistic studies in cell lines and activity in a mouse xenograft model in vivo.

Keywords: FLT3; cyclin-dependent kinase; purine; inhibitor; acute myeloid leukemia

check for updates

Citation: Tomanová, M.; Kozlanská, K.; Jorda, R.; Jedinák, L.; Havlíková, T.; Řezníčková, E.; Peřina, M.; Klener, P.; Dolníková, A.; Cankař, P.; et al. Synthesis and Structural Optimization of 2,7,9-Trisubstituted purin-8-ones as FLT3-ITD Inhibitors. *Int. J. Mol. Sci.* **2022**, *23*, 16169. https://doi.org/10.3390/ijms232416169

Academic Editor: George Mihai Nitulescu

Received: 30 November 2022
Accepted: 15 December 2022
Published: 18 December 2022

Publisher's Note: MDPI stays neutral with regard to jurisdictional claims in published maps and institutional affiliations.

1. Introduction

Acute myeloid leukemia (AML) is the most common type of acute leukemia in adults who have unfortunately poor prognosis and low survival rates. Approximately 30% of patients bear mutations in FMS-like tyrosine kinase 3 (FLT3), a transmembrane receptor kinase, which plays a key role in normal hematopoietic cell maturation, but its oncogenic activation results in the uncontrolled expansion of myeloid precursors. FLT3 can be activated by the internal tandem duplications (ITD) of the juxtamembrane domain or by point mutations in the kinase domain [1]. FLT3 mutation status relates to a prognosis, but it has also been validated as a drug target in AML and hematooncologists can now treat patients with newly approved drugs [2], including those based on small molecule kinase inhibitors, such as sorafenib, midostaurin, gilteritinib, crenolanib, or quizartinib (Figure 1) [1,3].

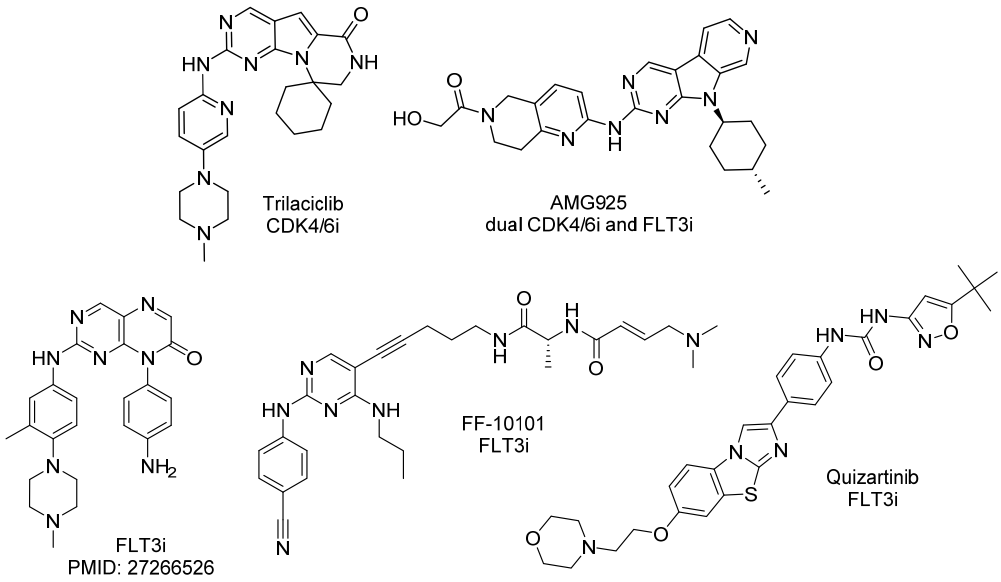

Figure 1. Example of inhibiting FLT3 kinase inhibitors.

Despite available targeted drugs, the therapy for FLT3-positive AML remains complicated due to the high rate of resistance to FLT3 inhibitors, often caused by changes in the kinase domain [4]. Various strategies to avoid reduced efficacy of therapy are explored, including combinations with conventional cytotoxics [2] or modern targeted drugs, such as BH3 mimetics [5,6], azacytidine [7], or kinase inhibitors [8–10]. Other approaches focus directly on the kinase realm by generating kinase inhibitors targeting resistance-causing FLT3 point mutations [11], or by developing dual targeting compounds, which inhibit FLT3 and another kinase necessary for survival and proliferation of AML cells, for example, JAK2, MEK, MER, or CDK4 [12].

One of these additional targets upregulated in AML is CDK4 [13], which is a key cell cycle regulating enzyme functioning downstream of FLT3. AML cells are sensitive to CDK4/6 inhibition [14,15]. In addition, the approved CDK4 inhibitor, trilaciclib, (Figure 1) also displays low nanomolar affinity to oncogenic variants of FLT3 [16]. In addition, several FLT3/CDK4 dual inhibitors (including clinical candidate AMG925) have been reported [17–20]. These compounds usually retain carbonyl function, which serves as a key hydrogen bond acceptor from D158 in CDK4. Carbonyl function in a corresponding position is also present in pteridin-7(8H)-one FLT3 inhibitor (Figure 1) [18]. In the current work, we have designed analogous 2,7,9-trisubstituted 8-oxopurines as FLT3 inhibitors and report here the structure-activity relationship (SAR) studies, which led to the discovery of compound **15a**. We also describe mechanistic studies in cell lines and activity in a mouse xenograft model in vivo.

2. Results and Discussion

2.1. Chemistry

The synthetic route to various purines **7**–**10** is described in Scheme 1. Reductive amination was used as a convenient method for the synthesis of derivatives **2** and **3** from commercially available pyrimidine **1**. Thus, we changed the typical reaction sequence to *N*-methyl pyrimidine **2**, where alkylation usually precedes to chlorination step [21]. In the case of **3**, we optimized reaction conditions using 2,2-dimethoxypropane and sodium triacetoxyborohydride [22].

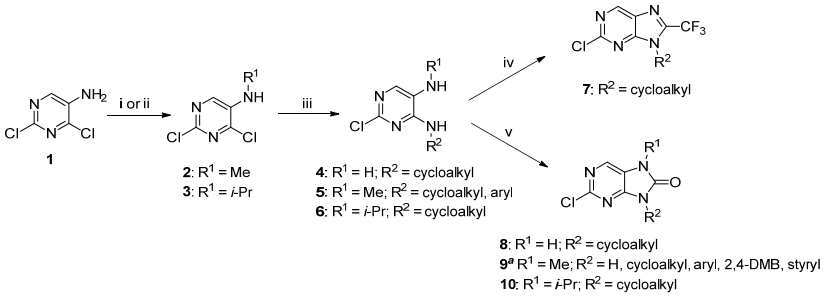

Scheme 1. Synthesis of intermediates for the Buchwald–Hartwig amination. (i) for R^1 = Me: 37% aq. HCHO, AcOH (conc.), $NaBH_3CN$, MeOH, 0–5 °C, 20 h; (ii) for R^1 = *i*-Pr: $(CH_3)_2C(OCH_3)_2$, AcOH (conc.), $NaBH(OAc)_3$, CH_2Cl_2, 0 °C—rt, 20 h; (iii) amine, DIEA, 85 °C, 48 h; (iv) TFAA, toluene, 70 °C, 16 h; (v) for R^1 = H, R^2 = cycloalkyl: $COCl_2$, 1 M LiHMDS in hexane, THF, −10 °C—rt. [a] Intermediate R^2 = H was obtained after deprotection of 2,4-DMB group with TFA in anisole at 90 °C for 18 h. Several intermediates R^2 = aryl, styryl were prepared using the Chan-Lam coupling reaction with aryl or styryl boronic acid, Cu_2S, TMEDA, in MeCN at rt for 24 h.

The further diverse step was the aromatic substitution of chloride at position 4 with various amines using *N*,*N*-diisopropylethylamine in butanol. Amines were subjected under our modified conditions [23], but some aromatic amines were more problematic. Noteworthy, only the desired position was involved in the substitution and no side products or hydrolysis were observed. *N*-methyl intermediate **2** was the most reactive toward aromatic nucleophilic substitution compared to an *N*-isopropyl one (**3**) or non-substituted amine **1**. In these cases, a longer reaction time or the addition of a base was needed.

Cyclization to purines **7** proceeded with trifluoroacetic anhydride and purinones **8**–**10** were isolated after reaction with a phosgene solution. Several aromatic and one styryl substituents were introduced using the Chan-Lam cross-coupling reaction using conditions from the literature [24], since the conventional method of aromatic nucleophilic substitution failed. 2-Methoxy, 4-methoxyphenyl, 2-tolyl, naphthyl, and styryl boronic acid were used as coupling partners with purinone intermediates **9** with the NH group at position 9. This intermediate was prepared easily after the deprotection of 2,4-dimethoxybenzyl group with TFA.

The Buchwald–Hartwig amination was used with piperazineaniline **11** to substitute the chlorine atom at position 2 (Scheme 2) since no general and high-yielded method for conventional aromatic nucleophilic substitution was found. The reaction was efficiently performed with precatalyst XPhos Pd G2 under microwave irradiation [25–27]. Only derivatives **13** with R^1 = H were more problematic. Prolongation of the reaction time from 1–2 to 6–9 h and an additional amount of the precatalyst solved the problem; however, deprotected purine **9** (R^2 = H) was still resistant to the coupling reaction. Finally, the Boc protecting group was removed to give a library of purines **12**–**15**; only a cleavage of the 2,4-DMB group required harsh conditions to get purine **14a**.

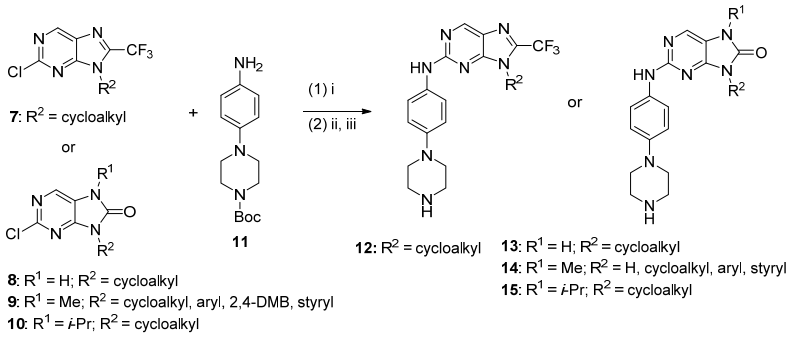

Scheme 2. Synthesis of target inhibitors. (i) XPhos Pd G2, K_2CO_3, 1,4-dioxane/H_2O (4:1), MW (150 W), 100 °C, 1–9 h; (ii) 36% HCl, CH_2Cl_2/MeOH (1:1), 48 h, (iii) for R^1 = Me, R^2 = H: TFA anisole, 90 °C, 5 days.

2.2. Kinase Inhibitory Activities—The SAR Study

Newly prepared compounds **12**–**15** were assayed for inhibition of FLT3-ITD kinase as well as CDK4 and CDK2, known off-targets of structurally related compounds. We observed that CDK4 was sensitive to nearly all compounds with IC_{50} values in mid-nanomolar values. Slight improvement in the anti-kinase potencies was observed with the increasing size of cycloalkyl moieties at position 9 (R2 substituent), namely from cyclopentyl to cycloheptyl. The substitution of the oxo for trifluoromethyl group at position 8 (derivatives **12a**–**12d**) dramatically improved inhibitory activities to all tested kinases to nanomolar values with slight preferences for CDK4 and FLT3. Compounds **13a**–**13d** having no substitution at position 7 of the purine ring did not display potency to the tested kinases.

The introduction of a methyl group at position **7** of the purine ring resulted in series **14**, which were prepared with diverse cycloalkyl and aryl substituents as R2. Our results showed the ability to affect the selectivity and, more importantly, the inhibitory activities of compounds because all compounds exceeded the activities of the unsubstituted derivative **14a**. An implementation of bulky substituents, namely cyclooctyl, cycloheptyl, 4-methylcyclohexyl, and cyclohexyl led to derivatives (**14i**, **14h**, **14g**, and **14e**, respectively) exhibiting all tested kinases with $IC_{50} \leq 300$ nM. Other derivatives bearing dodeka (**14j**), cyclopentyl (**14d**), 4-hydroxycyclohexyl (**14f**), 4-methylphenyl (**14o**), 4-methoxyphenyl (**14q**), and 4-fluorostyryl (**14t**) lost the CDK2 inhibitory potency ($IC_{50} > 1$ μM), while inhibition of CDK4 and FLT3 was preserved in mid-nanomolar values.

The introduction of phenyl and cyclobutyl substituents (**14m**, **14c**) showed to be important for FLT3 inhibition (IC_{50} = 50–60 nM), but led to a diminishing of activities against CDK4 (IC_{50} = 400–520 nM). Moreover, other derivatives with tetrahydropyranyl (**14k**), 2,4-dimethoxybenzyl (**14r**), cyclopropyl (**14b**), and naphthyl (**14s**) exhibited similar specificity for FLT3 kinase over CDK4 and CDK2 ($IC_{50} > 1$ μM), but the IC_{50} values for FLT3 dropped to mid-nanomolar values.

Finally, we explored the activities of four compounds that possess an isopropyl substituent at position 7 and cyclopentyl, cyclohexyl, 4-methylcyclohexyl, or cycloheptyl groups (**15a**–**15d**) at position 9 of the purine ring. All these derivatives displayed interesting activities for FLT3 kinase (IC_{50} = 30–70 nM) and selectivity over tested CDKs. Comparison with counterparts differing in the methyl and isopropyl moieties (pairs **15d** and **14h**, **15a** and **14d**, **15c** and **14g**, and **15b** and **14e**) indicates that isopropyl markedly contributes to selectivity against FLT3.

2.3. Kinase Selectivity

Three representative compounds (**14d**, **14e**, and **15a**) were profiled in a 1 μM concentration against 30 kinases that were selected as known off-targets of approved CDK4/6 inhibitors [28]. Compounds **14d** and **14e**, differing only in the cyclopentyl and cyclohexyl moiety at position **9** of the purine ring, were confirmed to be potent CDK4 and FLT3 inhibitors (Figure S1). Additional sensitive kinases include STK16, EphA1, MEKK2, SRC, and MER (≤10% of residual enzyme activities), which are not targets of the structurally similar CDK4/6 inhibitor, trilaciclib. We also screened compound **15a**, an analogue of **14d**, bearing isopropyl at position 7 of the purine instead of the methyl group. This change rapidly diminished the potency against CDK4 (dropped to 90% of residual enzyme activity), but the preference for FLT3 remained (1st rank) (Figure 2). Further, four kinases, namely Src, TTK, Lyn, and Abl were also potently inhibited (≤10% of residual activities).

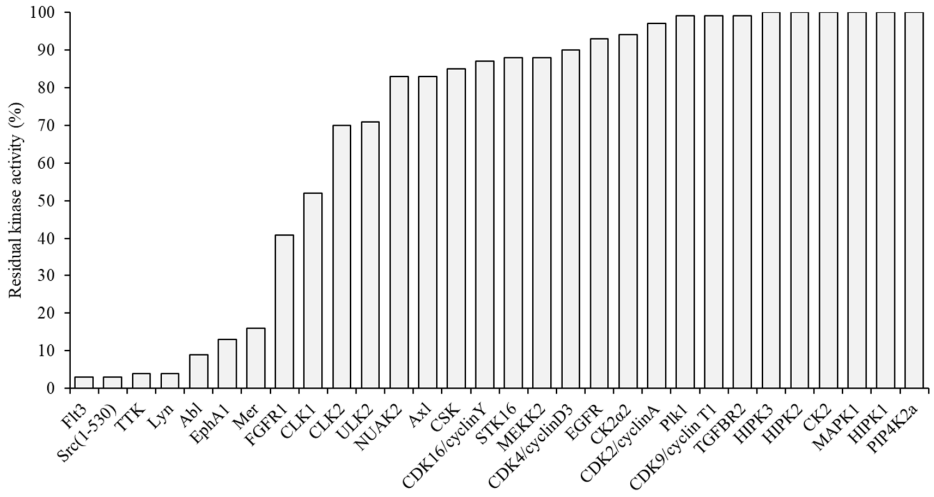

Figure 2. Kinase selectivity profiles of **15a** assayed at 1 μM concentration.

2.4. Binding of 15a in the FLT3 Active Site

Molecular docking of **15a** into the FLT3 in active conformation (DFG-in) [29] proposed plausible binding in the active site in a manner corresponding to known inhibitors of CDK4, CDK6, and FLT3 [30,31] (Figure 3). The orientation of the compound is consistent with type I binding. In the hinge region, two putative conserved hydrogen bonds are formed between the backbone of Cys694 and **15a**. The isopropyl in position 7 of purine core can make extensive hydrophobic interactions with Val624, Lys644, Val675, Leu 767, and the gatekeeper, Phe691. The cyclopentyl ring forms hydrophobic contacts with Asp698 and Leu767.

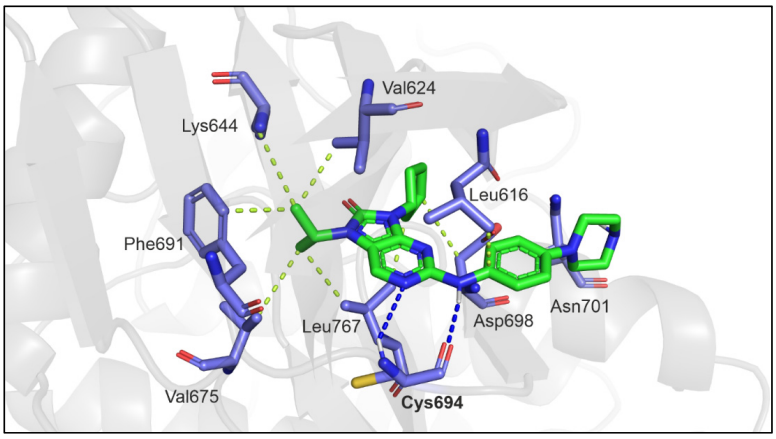

Figure 3. Binding pose of **15a** (green sticks) in the model of FLT3. The kinase is shown in gray with interacting residues shown as blue sticks. Heteroatoms are blue (nitrogens), red (oxygens), yellow (sulfur), and white (hydrogens).

2.5. Antiproliferative Properties of Prepared Compounds

In parallel to kinase assays, we measured the effect of compounds on the viability of cancer cell lines MV4-11 and K562 using a resazurin-based assay. MV4-11 is an AML cell line dependent on a constitutively activated FLT3-ITD kinase with high sensitivity to FLT3 inhibition, K562 cells (chronic myelogenous leukemia) are independent on FLT3. As shown in Table 1, most of the compounds have GI_{50} values in a mid-nanomolar range in MV4-11 cells, while K562 cells were substantially less sensitive (most of GI_{50} > 1 μM). Eleven compounds displayed GI_{50} below 200 nM in MV4-11 and from these, compounds **14i** and **14e** exerted a selectivity index > 20 (ratio for GI_{50}'s of K562 and MV4-11 cells). Compound **15a** was the most potent in MV4-11 cells expressing GI_{50} = 50 nM.

Table 1. Antiproliferative and kinase inhibitory potencies of novel compounds.

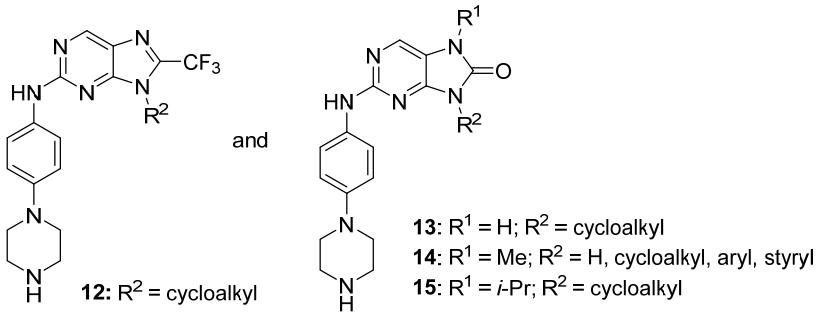

			GI_{50} (μM) *		IC_{50} (μM) *		
Cmpd.	**R^1**	**R^2**	**MV4-11**	**K562**	**CDK2/E**	**CDK4/D1**	**FLT3-ITD**
12a	-	cyclopentyl	0.22	1.11	1.63	0.051	0.224
12b	-	cyclohexyl	0.11	1.17	0.23	0.016	0.060
12c	-	4-methylcyclohexyl	0.44	8.21	0.23	0.012	0.085
12d	-	cycloheptyl	0.25	2.45	0.15	0.022	0.088
13a	-H	cyclopentyl	0.68	1.63	24.5	2.885	2.366
13b	-H	cyclohexyl	0.69	1.78	3.36	0.782	1.592
13c	-H	4-methylcyclohexyl	0.70	1.9	2.56	0.451	1.047
13d	-H	cycloheptyl	0.56	1.58	1.00	0.479	0.425
14a	methyl	-H	5.65	>100	>20	>20	6.90
14b	methyl	cyclopropyl	0.71	45.3	>20	8.02	0.642
14c	methyl	cyclobutyl	0.11	1.04	3.90	0.524	0.056
14d	methyl	cyclopentyl	0.12	0.96	1.82	0.157	0.083
14e	methyl	cyclohexyl	0.20	4.53	0.30	0.020	0.068
14f	methyl	4-hydroxycyclohexyl	0.51	9.37	2.87	0.250	0.132
14g	methyl	4-methylcyclohexyl	0.11	1.26	0.18	0.027	0.068
14h	methyl	cycloheptyl	0.10	1.48	0.06	0.022	0.034
14i	methyl	cyclooctyl	0.09	2.46	0.09	0.025	0.012
14j	methyl	dodeka	1.81	3.59	1.02	0.338	0.075
14k	methyl	tetrahydropyranyl	0.59	18.2	9.25	2.53	0.450
14l	methyl	4-methylpiperidin	1.72	31.6	15.8	>20	2.85
14m	methyl	phenyl	0.34	3.03	3.74	0.40	0.054
14n	methyl	2-methylphenyl	1.25	16.7	0.54	1.87	2.94
14o	methyl	4-methylphenyl	0.46	7.62	2.40	0.169	0.160
14p	methyl	2-methoxyphenyl	0.31	0.37	1.59	2.72	0.306
14q	methyl	4-methoxyphenyl	0.40	1.97	6.18	0.488	0.262
14r	methyl	2,4-dimethoxybenzyl	0.90	11.9	20.0	>20	0.456
14s	methyl	naphtyl	0.33	2.53	9.53	6.90	0.850
14t	methyl	4-fluorostyryl	0.52	2.29	7.7	0.216	0.345
15a	isopropyl	cyclopentyl	0.05	0.58	5.06	1.90	0.037
15b	isopropyl	cyclohexyl	0.13	1.51	10.3	2.12	0.068
15c	isopropyl	4-methylcyclohexyl	0.13	1.45	4.14	1.10	0.040
15d	isopropyl	cycloheptyl	0.10	1.18	2.32	1.10	0.027

* all data were obtained from at least duplicate experiments.

FLT3 inhibition causes G1-cell cycle arrest in FLT3-dependent cell lines such as MV4-11; we, therefore, performed flow cytometric analysis to evaluate cell cycle changes in MV4-11 and K562 cell lines treated with 200 nM compounds for 24 h. The data showed that most compounds block the cell cycle in the G1 phase in MV4-11 cells. Specifically, 18 compounds arrested >85% of cells in the G1 phase, which is >30% cells in the G1 phase of the cell cycle than in control cells (Figure 4A). The observed results confirmed the data obtained from the viability assays because all non-toxic compounds (e.g., **14a**, **14j**, **14l**, and **14n**) did not significantly affect the cell cycle in MV4-11 cells. No changes in cell cycle distribution upon treatment were observed in K562 cells, confirming the specificity of the compounds (Figure 4B). Only a few compounds, such as **12c**, **14e**, and **14g**–**14i**, caused moderate G1 block in K562 that probably stems from the potent inhibition of CDK4 (see Table 1). The control experiments were performed with palbociclib and quizartinib; palbociclib could significantly arrest both cell lines in the G1 phase, while quizartinib arrested selectively only MV4-11.

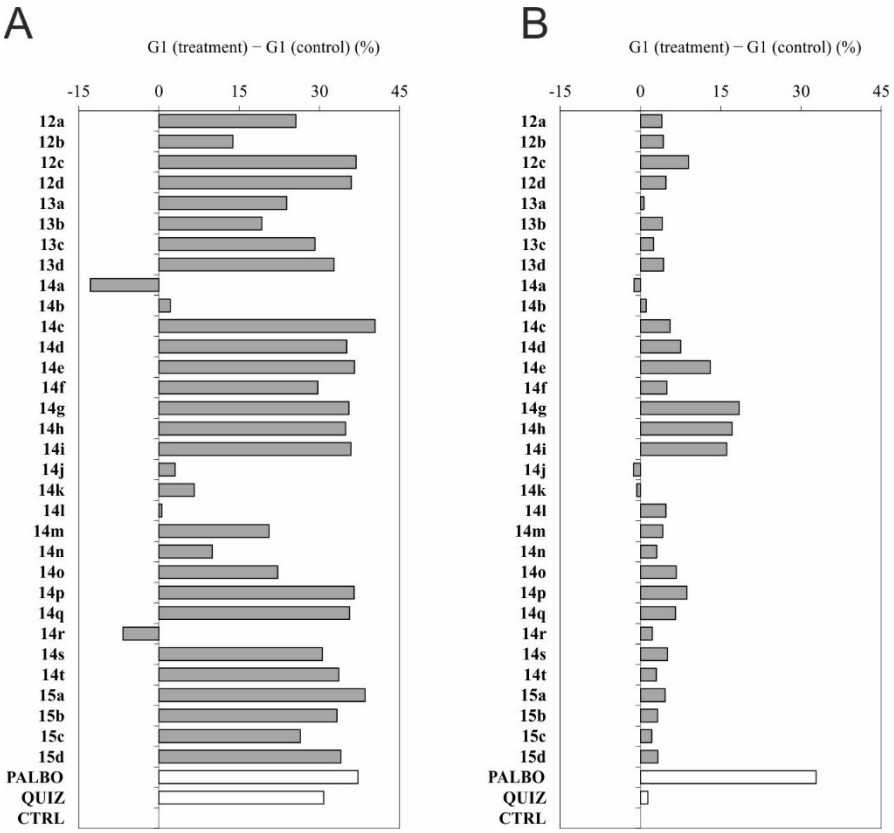

Figure 4. Cell cycle G1 phase population upon treatment of MV4-11 (**A**) and K562 (**B**) cells with a 200 nM concentration for 24 h. Data (in %) are expressed as differences between G1 populations in treated and control cells. PALBO, palbociclib; QUIZ, quizartinib.

Finally, we performed flow cytometric analysis with different concentrations of **15a** in MV4-11 and MOLM13 (another FLT-ITD positive cell line) and K562 cell lines treated for 24 h (Figure 5). Increasing doses of **15a** arrested cells in the G1 phase of the cell cycle up to 90% which was also observed for the FLT3 inhibitor, quizartinib. Oppositely, cell line K562 did not show any changes upon treatment with **15a** and quizartinib.

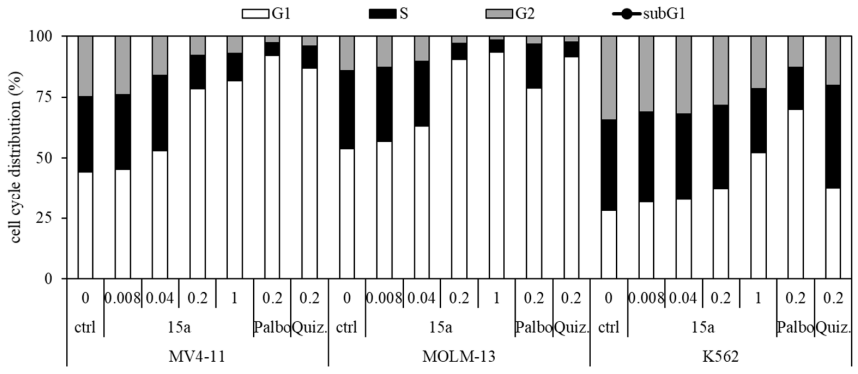

Figure 5. Cell cycle distribution of MV4-11, MOLM-13 and K562 cells treated with different concentrations of **15a** for 24 h. Quiz., quizartinib; Palbo, palbociclib.

2.6. Inhibition of FLT3 Signaling In Vivo

Next, we investigated the compounds for their ability to inhibit FLT3 and its downstream signaling in the MV4-11 cell line. Western blot analysis after 1 h treatment of MV4-11 cells revealed that **14e** inhibits autophosphorylation of FLT3 kinase at Y589/591 and subsequently diminishes the phosphorylation of its downstream proteins, STAT5 and

ERK1/2, in nanomolar doses (Figure 6). A similar inhibitory pattern was observed in quizartinib-treated cells.

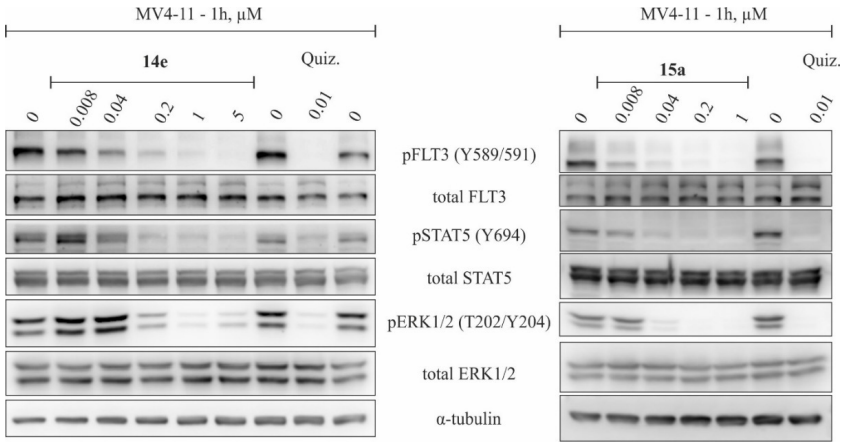

Figure 6. Effect of **14e** and **15a** on phosphorylation of FLT3 and its downstream signaling pathways. MV4-11 cells were treated for 1 h with indicated concentrations of the compounds; quizartinib (Quiz.) was used as a standard. α-tubulin was used for equal protein loading.

In parallel, we examined the effect of the most potent and selective FLT3 inhibitor **15a**, which showed a similar inhibitory pattern of signalling inhibition. The dephosphorylation of FLT3 was observed already at an 8 nM concentration and nearly complete suppression of ERK1/2 at 40 nM of **15a**.

2.7. In Vivo Activity of 15a in MV4-11 Xenograft Model

Finally, we tested the in vivo activity of **15a** in a model of AML based on subcutaneous xenotransplantation of MV4-11 cells in immunodeficient mice. As shown in Figure 7A, daily i.p. treatment with **15a** (20 mg/kg) was associated with a significant reduction in the growth of xenografted MV4-11 cells compared to vehicle-dosed control mice. Importantly, no significant reduction in mice weight was observed during the therapy (Figure 7B).

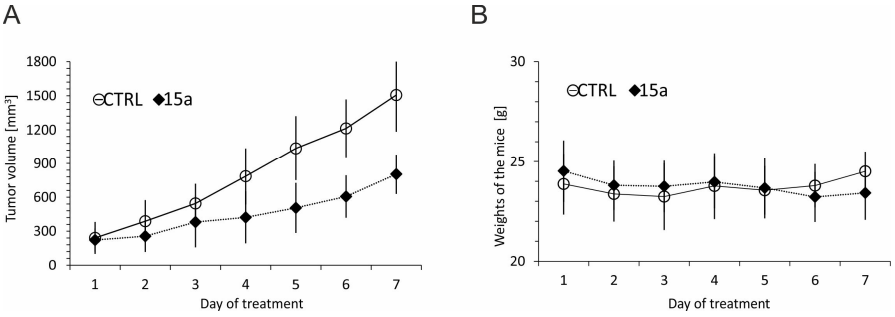

Figure 7. Calculated tumor growth curves (**A**) and mice weight (**B**) in MV4-11 xenografted mice treated with **15a**.

3. Materials and Methods

3.1. General Information

Starting materials and reagents were purchased from various commercial sources (VWR, Radnor, PA, USA; Merck, Darmstadt, Germany; Fluorochem, Hadfield, UK; Acros Organics, Waltham, MA, USA) and used as received. All reactions were carried out under air. Reaction workup and column chromatography were performed with commercial grade solvents without further purification. All reactions were monitored using LC/MS analysis or thin-layer chromatography (TLC) using aluminium plates precoated with silica gel (silica gel 60 F254, Merck, US) impregnated with a fluorescent indicator. TLC plates were visualized using exposure to ultraviolet light (λ = 254 nm). Flash chromatography

was performed using silica gel (35–70 μm partical size) column chromatography. The cross-coupling reactions under microwave irradiation were performed in a 10 mL glass tube sealed with a PTFE coated septa. Reaction mixture was pre-mixed for 1 min with rapid stirring and then irradiated at a maximum power of 150 W with simultaneous cooling using compressed air (24 psi). When the desired temperature was reached (ramping time ∼1 min), the power was automatically adjusted to maintain the set reaction temperature for a specified time. Finally, the vessel was cooled to approximately 40 °C with compressed air (cooling time ∼1 min). Intermediates **2**, **3**, **4a**, **4b**, **5c**, **8a**–**b**, **9c**–**e**, **9j**, and **9l**, **9p**–**o** have been already reported [21,22,32–35], for more information see Supplementary Information.

3.2. Instrumentation

The LC−MS analyses were carried out using UPLC Waters Acquity equipped with PDA and QDa detectors. The system comprised XSelect HSS T3 (Waters, Milford, MA, USA) 3 mm × 50 mm C18 reverse phase column XP, 2.5 μm particles. Mobile phases: 10 mM ammonium acetate in HPLC grade water (A) and gradient grade acetonitrile for HPLC (B). A gradient was mainly formed from 20 to 80% of B in 4.5 min, kept for 1 min, with a flow rate of 0.6 mL/min. The MS ESI operated at a 25 V cone voltage, 600 °C probe temperature, and a 120 °C source temperature.

All ^{1}H and ^{13}C NMR experiments were performed at magnetic field strengths of 11.75 T (with operating frequencies 500.16 MHz for ^{1}H and 125.77 MHz for ^{13}C) and 9.39 T (with operating frequencies 399.78 MHz for ^{1}H and 100.53 MHz for ^{13}C) at an ambient temperature (20 °C). ^{1}H and ^{13}C spectra were referenced relative to the signal of DMSO-d_6 (^{1}H: δ = 2.50 ppm, ^{13}C: δ = 39.51 ppm) or $CDCl_3$ (^{1}H: δ = 7.260 ppm, ^{13}C: δ = 77.160 ppm).

HRMS analyses were performed using UPLC Dionex Ultimate 3000 equipped with an Orbitrap Elite high-resolution mass spectrometer, Thermo Exactive plus, operating at full scan mode (120,000 FWMH) in the range of 100−1800 m/z. The settings for electrospray ionization were as follows: oven temperature of 150 °C and a source voltage of 3.6 kV. The acquired data were internally calibrated with diisooctyl phthalate as a contaminant in MeOH (m/z 391.2843).

Melting points were determined using VEB Analytik Dresden PHMK 78/1586 apparatus. Microwave experiments were conducted in the CEM Discover SP closed vessel microwave synthesizer.

3.3. General Synthetic Procedure 1: Pyrimidine-4,5-Diamines Formation

To a solution of **1**, **2**, or **3** (1.00 mmol) in butanol (10 mL), corresponding amine (1.00 mmol) and *N*,*N*-diisopropylethylamine (259 mg, 348 μL, and 2.00 mmol) were added. The reaction mixture was heated at 85 °C for 48 h. Then, butanol was evaporated under reduced pressure and the crude product was purified using column chromatography (usually 1:1 hexane/EtOAc).

3.4. General Synthetic Procedure 2: Cyclization with TFAA

For compound **4**, 0.75 mmol was put into a flask, and toluene (1 mL) and trifluoroacetic anhydride (3 mL) were added. The mixture was heated at 70 °C for 16 h. The crude mixture was diluted with dichloromethane (20 mL), then washed with 10% K_2CO_3 (30 mL) and distilled water (30 mL), and dried over $MgSO_4$. The solvent was evaporated under reduced pressure (rotovap) and the residue was purified using column chromatography (usually 5:1 hexane/EtOAc).

3.5. General Synthetic Procedure 3: Cyclization with Phosgene

For compounds **4**, **5**, or **6**, 0.70 mmol was dissolved in anhydrous THF (10 mL) under inert atmosphere of nitrogen and cooled to −10 °C. After the slow addition of 15 wt % $COCl_2$ in toluene (560 μL, 0.85 mmol), 1 M LiHMDS in hexane (1.4 mL, 1.40 mmol) was added portionwise. After 1 h, the reaction mixture was cooled to ambient temperature

and stirred for 20 min. The mixture was then evaporated under reduced pressure and the residue was purified using column chromatography (usually 2:1 EtOAc/hexane).

3.6. Preparation of Intermediate 9 (R^1 = Me, R^2 = H)

2-Chloro-9-(2,4-dimethoxybenzyl)-7-methyl-7,9-dihydro-8*H*-purin-8-one (200 mg, 0.59 mmol) was suspended in anisole (3.15 mL) and TFA (2.6 mL) was added. The reaction mixture was stirred at 90 °C for 18 h. TFA was evaporated using the flow of nitrogen and anisole was evaporated using RVO. A crude mixture was dissolved in MeOH, and solid $NaHCO_3$ was added to neutralize the mixture and evaporated with silica gel. The product was purified using column chromatography (4:1 to 2:1 hexane/EtOAc). After evaporation and trituration with diethylether, the product was filtered-off to yield 2-chloro-7-methyl-7,9-dihydro-8*H*-purin-8-one 56 mg (52 %) as a white solid.

3.7. General Synthetic Procedure 4: Chan-Lam Cross-Coupling Reaction

A 10 mL vial was charged with Cu_2S (8 mg, 0.05 mmol), MeCN (0.6 mL), and *N*,*N*,*N*′,*N*′-tetramethylethane-1,2-diamine (30 µL, 0.20 mmol). After 1 h of stirring, 2-chloro-7-methyl-7,9-dihydro-8*H*-purin-8-one (18 mg, 0.10 mmol) and boronic acid (0.20 mmol) were added and the mixture was stirred at ambient temperature for 24 h. A crude mixture was loaded on Celite, evaporated using RVO, and purified using column chromatography (2:1 hexane/EtOAc).

3.8. General Synthetic Procedure 5: Buchwald–Hartwi Amination and Boc Deprotection

A microwave vial was charged with **7**, **8**, **9**, or **10** (0.25 mmol), 1 mL of mixture 1,4-dioxane/H_2O (4:1), *tert*-butyl 4-(4-aminophenyl)piperazine-1-carboxylate (55.4 mg, 0.20 mmol), K_2CO_3 (138 mg, 1.00 mmol), and XPhos Pd G2 (4 mg, 2 mol%). The reaction mixture was heated at 100 °C under microwave irradiation for 1–9 h, the end of the reaction was monitored using HPLC/MS. The mixture was evaporated under reduced pressure and purified using column chromatography (1:1 hexane/EtOAc). All prepared Boc-protected intermediates (0.15 mmol) were dissolved in 2.8 mL of DCM/MeOH (1:1) and 36% HCl (240 µL) was added. After full conversion (checked using HPLC-MS; approximately 48 h), 1 mL of distilled water was added together with solid K_2CO_3 to neutralize the mixture. Solvents were evaporated and the product was purified using column chromatography (10:1 DCM/MeOH).

3.9. Cell Cultures and Viability Assay

Human cell lines were obtained from the European Collection of Authenticated Cell Cultures (K562) and Cell lines service (MV4-11) and were cultivated according to the provider's instructions. Briefly, cells were maintained in RPMI-1640 (MV4-11) or DMEM (K562) supplemented with 10% fetal bovine serum, penicillin (100 U/mL), and streptomycin (0.1 mg/mL) at 37 °C in 5% CO_2. For the viability assays, cells were treated in triplicate with six different doses of each compound for 72 h. After treatments, the resazurin (Sigma Aldrich, St. Louis, MO, USA) solution was added for 4 h, and the fluorescence of resorufin corresponding to live cells was measured at 544/590 nm (excitation/emission) using a Fluoroskan Ascent microplate reader (Labsystems). The GI_{50} value, the drug concentration lethal to 50% of the cells, was calculated from the dose-response curves that resulted from the assays.

3.10. Kinase Inhibition Assays

CDK/cyclin complexes and FLT3 kinases were assayed as previously described [36,37]. Protein kinase selectivity was evaluated at a single concentration (1 µM) by screening against 30 enzymes at Eurofins Discovery (France).

3.11. Immunoblotting

Cell lysates were prepared, and then proteins were separated on SDS-polyacrylamide gels and electroblotted onto nitrocellulose membranes. After blocking, overnight incubation with specific primary antibodies, and incubation with peroxidase-conjugated secondary antibodies, peroxidase activity was detected with Super-Signal West Pico reagents (Thermo Scientific, Waltham, MA, USA) using a CCD camera LAS-4000 (Fujifilm, Minato, Japan). The specific antibodies were purchased from Cell signaling (anti-FLT3, clone 8F2; anti-phospho-FLT3 Y589/591, clone 30D4; anti-STAT5; anti-phospho-STAT5 Y694; anti-ERK1/2; anti-phospho-ERK1/2 T202/Y204; and peroxidase-conjugated secondary antibodies) or Merck (anti-α-tubulin, clone DM1A)

3.12. Flow Cytometry

Asynchronously growing cells were seeded into a 96-well plate and, after a preincubation period, treated with tested compounds for 24 h. The treated cells were stained directly (or after trypsinization for the adherent cells) with the 5× staining solution (17 mM trisodium citrate dihydrate, 0.5% IGEPAL CA-630, 7.5 mM spermine tetrahydrochloride, and 2.5 mM Tris; pH 7.6 containing 50 mg/mL propidium iodide). After the staining, DNA content was analyzed using flow cytometry using a 488 nm laser (BD FACS Verse with software BD FACSuite™, version 1.0.6). Cell cycle distribution was analyzed using ModFit LT (Verity Software House, version 5.0). Palbociclib, trilaciclib, and quizartinib were purchased from MedChemExpress, Monmouth Junction, NJ, USA.

3.13. Molecular Docking

Molecular docking was performed into the previously published model of FLT3 in the active conformation [29]. The 3D structure of **15a** and the conformations with the lowest energy were obtained using molecular mechanics with Avogadro 1.90.0. Polar hydrogens were added to ligand and protein with the AutoDock Tools program and rigid docking was performed using AutoDock Vina 1.059 [38]. Interactions between **15a** and FLT3 were determined using PLIP (protein–ligand interaction profiler) [39] and the figure was generated using Pymol ver. 2.0.4 (Schrödinger, LLC, New York, NY, USA).

3.14. Experimental Therapy

The experimental design was approved by the Institutional Animal Care and Use Committee (MSMT-37334/2020-4). Immunodeficient adult female NOD.Cg-*Prkdc*^{scid}*Il2rg*^{tm1Wjl}/SzJ mice (referred to as NSG mice) were purchased from The Jackson Laboratory and preserved in a pathogen-free environment in individually ventilated cages, provided with sterilized food and water. NSG mice were subcutaneously inoculated with 10×10^6 leukemia cells. After all mice developed palpable tumors, they were stratified into cohorts with comparable tumor volumes and therapy with **15a** (20 mg/kg, daily i.p. dosing, 7 consecutive days) was initiated (=day 1, D1). Each cohort contained 6 animals. Three perpendicular dimensions (in millimeters) were measured daily with a digital caliper and tumor volumes were calculated using the following formula: $\pi/6 \times$ length $\times$ width $\times$ height. An experiment was terminated (and mice euthanized) when tumors exceeded 20 mm in the largest diameter.

4. Conclusions

In summary, we prepared a series of 2,7,9-trisubstituted-purin-8-nones to compare structure-activity relationships on CDK2, CDK4, and FLT3 kinases. It was revealed that FLT3 kinase was more tolerant in the structural variety of substituents at positions 7 and 9 than CDK4 kinase. The introduction of the isopropyl group at position 7 was significantly beneficial for selectivity toward FLT3 kinase. The more detailed selectivity study on 30 kinases, known as off-targets of approved CDK4/6 inhibitors, with three representative compounds showed effective inhibition of four additional kinases STK16, TTK, NUAK2, Lyn, and Src. Cellular analyses with MV4-11 cells treated the selected candidates **14e** and **15a** confirmed the inhibition of autophosphorylation of FLT3 kinase, subsequent

dephosphorylation of the downstream proteins STAT5 and ERK1/2 in nanomolar doses, and G1-cell cycle arrest. The pharmacological properties of the model compound studied on Caco-2 cells indicated a substantially higher stability of inhibitor **14e** in comparison with trilaciclib. To our delight, a significant reduction in tumor growth was observed during the therapy of the MV4-11 xenograft model.

Supplementary Materials: The following supporting information can be downloaded at: https://www.mdpi.com/article/10.3390/ijms232416169/s1.

Author Contributions: Synthesis, analytical data processing, writing, M.T.; synthesis, methodology, T.H. and L.J.; writing—original draft preparation, R.J., M.T.; biochemistry and biology, investigation, K.K., E.Ř., P.K., A.D.; docking, M.P.; conceptualization, supervision, project administration, funding acquisition, V.K., P.C. All authors have read and agreed to the published version of the manuscript.

Funding: The work was supported by the European Union—Next Generation EU (The project National Institute for Cancer Research, Programme EXCELES, ID No. LX22NPO5102), Czech Science Foundation (20-25308S and 21-06553S), the Ministry of Health of the Czech Republic (NV19-08-00144) and Palacký University Olomouc (IGA_PrF_2022_007 and IGA_PrF_2022_022).

Institutional Review Board Statement: The animal study protocol was approved by the Institutional Animal Care and Use Committee (Charles University in Prague).

Data Availability Statement: All data are reported in the manuscript and in the Supplementary Material and are available from the corresponding authors upon request.

Acknowledgments: We would like to thank Jana Hudcová and Veronika Vojáčková for technical assistance. Plasmids for the expression of CDK2 and cyclin A2 were kindly gifted by Daniel Fisher (IGMM, CNRS, Montpellier, France).

Conflicts of Interest: The authors declare no conflict of interest.

References

1. Daver, N.; Schlenk, R.F.; Russell, N.H.; Levis, M.J. Targeting FLT3 mutations in AML: Review of current knowledge and evidence. *Leukemia* **2019**, *33*, 299–312. [CrossRef] [PubMed]
2. Kayser, S.; Levis, M.J. Updates on targeted therapies for acute myeloid leukaemia. *Br. J. Haematol.* **2022**, *196*, 316–328. [CrossRef] [PubMed]
3. Ahn, J.S.; Kim, H.J. FLT3 mutations in acute myeloid leukemia: A review focusing on clinically applicable drugs. *Blood Res.* **2022**, *57*, 32–36. [CrossRef] [PubMed]
4. Scholl, S.; Fleischmann, M.; Schnetzke, U.; Heidel, F.H. Molecular Mechanisms of Resistance to FLT3 Inhibitors in Acute Myeloid Leukemia: Ongoing Challenges and Future Treatments. *Cells* **2020**, *9*, 2493. [CrossRef]
5. Ma, J.; Zhao, S.; Qiao, X.; Knight, T.; Edwards, H.; Polin, L.; Kushner, J.; Dzinic, S.H.; White, K.; Wang, G.; et al. Inhibition of Bcl-2 Synergistically Enhances the Antileukemic Activity of Midostaurin and Gilteritinib in Preclinical Models of FLT3-Mutated Acute Myeloid Leukemia. *Clin. Cancer Res.* **2019**, *25*, 6815–6826. [CrossRef]
6. Zhu, R.; Li, L.; Nguyen, B.; Seo, J.; Wu, M.; Seale, T.; Levis, M.; Duffield, A.; Hu, Y.; Small, D. FLT3 tyrosine kinase inhibitors synergize with BCL-2 inhibition to eliminate FLT3/ITD acute leukemia cells through BIM activation. *Signal. Transduct. Target Ther.* **2021**, *6*, 186. [CrossRef]
7. Ohanian, M.; Garcia-Manero, G.; Levis, M.; Jabbour, E.; Daver, N.; Borthakur, G.; Kadia, T.; Pierce, S.; Burger, J.; Richie, M.A.; et al. Sorafenib Combined with 5-azacytidine in Older Patients with Untreated FLT3-ITD Mutated Acute Myeloid Leukemia. *Am. J. Hematol.* **2018**, *93*, 1136–1141. [CrossRef]
8. Djamai, H.; Berrou, J.; Dupont, M.; Kaci, A.; Ehlert, J.E.; Weber, H.; Baruchel, A.; Paublant, F.; Prudent, R.; Gardin, C.; et al. Synergy of FLT3 inhibitors and the small molecule inhibitor of LIM kinase1/2 CEL_Amide in FLT3-ITD mutated Acute Myeloblastic Leukemia (AML) cells. *Leuk. Res.* **2021**, *100*, 106490. [CrossRef]
9. Inaba, H.; van Oosterwijk, J.G.; Panetta, J.C.; Li, L.; Buelow, D.R.; Blachly, J.S.; Shurtleff, S.; Pui, C.H.; Ribeiro, R.C.; Rubnitz, J.E.; et al. Preclinical and Pilot Study of Type I FLT3 Tyrosine Kinase Inhibitor, Crenolanib, with Sorafenib in Acute Myeloid Leukemia and FLT3-Internal Tandem Duplication. *Clin. Cancer Res.* **2022**, *28*, 2536–2546. [CrossRef]
10. Qiao, X.; Ma, J.; Knight, T.; Su, Y.; Edwards, H.; Polin, L.; Li, J.; Kushner, J.; Dzinic, S.H.; White, K.; et al. The combination of CUDC-907 and gilteritinib shows promising in vitro and in vivo antileukemic activity against FLT3-ITD AML. *Blood Cancer J.* **2021**, *11*, 111. [CrossRef]
11. Yamaura, T.; Nakatani, T.; Uda, K.; Ogura, H.; Shin, W.; Kurokawa, N.; Saito, K.; Fujikawa, N.; Date, T.; Takasaki, M.; et al. A novel irreversible FLT3 inhibitor, FF-10101, shows excellent efficacy against AML cells with FLT3 mutations. *Blood* **2018**, *131*, 426–438. [CrossRef] [PubMed]

12. Yuan, T.; Qi, B.; Jiang, Z.; Dong, W.; Zhong, L.; Bai, L.; Tong, R.; Yu, J.; Shi, J. Dual FLT3 inhibitors: Against the drug resistance of acute myeloid leukemia in recent decade. *Eur. J. Med. Chem.* **2019**, *178*, 468–483. [CrossRef] [PubMed]
13. Drexler, H.G. Review of alterations of the cyclin-dependent kinase inhibitor INK4 family genes p15, p16, p18 and p19 in human leukemia-lymphoma cells. *Leukemia* **1998**, *12*, 845–859. [CrossRef] [PubMed]
14. Uras, I.Z.; Walter, G.J.; Scheicher, R.; Bellutti, F.; Prchal-Murphy, M.; Tigan, A.S.; Valent, P.; Heidel, F.H.; Kubicek, S.; Scholl, C.; et al. Palbociclib treatment of FLT3-ITD+ AML cells uncovers a kinase-dependent transcriptional regulation of FLT3 and PIM1 by CDK6. *Blood* **2016**, *127*, 2890–2902. [CrossRef]
15. Wang, L.; Wang, J.; Blaser, B.W.; Duchemin, A.M.; Kusewitt, D.F.; Liu, T.; Caligiuri, M.A.; Briesewitz, R. Pharmacologic inhibition of CDK4/6: Mechanistic evidence for selective activity or acquired resistance in acute myeloid leukemia. *Blood* **2007**, *110*, 2075–2083. [CrossRef]
16. Bisi, J.E.; Sorrentino, J.A.; Jordan, J.L.; Darr, D.D.; Roberts, P.J.; Tavares, F.X.; Strum, J.C. Preclinical development of G1T38: A novel, potent and selective inhibitor of cyclin dependent kinases 4/6 for use as an oral antineoplastic in patients with CDK4/6 sensitive tumors. *Oncotarget* **2017**, *8*, 42343–42358. [CrossRef]
17. Li, C.; Liu, L.; Liang, L.; Xia, Z.; Li, Z.; Wang, X.; McGee, L.R.; Newhall, K.; Sinclair, A.; Kamb, A.; et al. AMG 925 is a dual FLT3/CDK4 inhibitor with the potential to overcome FLT3 inhibitor resistance in acute myeloid leukemia. *Mol. Cancer Ther.* **2015**, *14*, 375–383. [CrossRef]
18. Sun, D.; Yang, Y.; Lyu, J.; Zhou, W.; Song, W.; Zhao, Z.; Chen, Z.; Xu, Y.; Li, H. Discovery and Rational Design of Pteridin-7(8H)-one-Based Inhibitors Targeting FMS-like Tyrosine Kinase 3 (FLT3) and Its Mutants. *J. Med. Chem.* **2016**, *59*, 6187–6200. [CrossRef]
19. Li, X.; Yang, T.; Hu, M.; Yang, Y.; Tang, M.; Deng, D.; Liu, K.; Fu, S.; Tan, Y.; Wang, H.; et al. Synthesis and biological evaluation of 6-(pyrimidin-4-yl)-1H-pyrazolo[4,3-b]pyridine derivatives as novel dual FLT3/CDK4 inhibitors. *Bioorg. Chem.* **2022**, *121*, 105669. [CrossRef]
20. Wang, Y.; Zhi, Y.; Jin, Q.; Lu, S.; Lin, G.; Yuan, H.; Yang, T.; Wang, Z.; Yao, C.; Ling, J.; et al. Discovery of 4-((7H-Pyrrolo[2,3-d]pyrimidin-4-yl)amino)-N-(4-((4-methylpiperazin-1-yl)methyl)phenyl)-1H-pyrazole-3-carboxamide (FN-1501), an FLT3- and CDK-Kinase Inhibitor with Potentially High Efficiency against Acute Myelocytic Leukemia. *J. Med. Chem.* **2018**, *61*, 1499–1518. [CrossRef]
21. Huang, Z.; Zhang, Q.; Yan, L.; Zhong, G.; Zhang, L.; Tan, X.; Wang, Y. Approaching the active conformation of 1,3-diaminopyrimidine based covalent inhibitors of Bruton's tyrosine kinase for treatment of Rheumatoid arthritis. *Bioorganic Med. Chem. Lett.* **2016**, *26*, 1954–1957. [CrossRef] [PubMed]
22. Jin, B.; Scorah, N.; Dong, Q. Hexahydrooxazinopterine Compounds for Use as mTOR Inhibitors. WO2011025889A1, 3 March 2011.
23. Vijay, K.D.; Hoarau, C.; Bursavich, M.; Slattum, P.; Gerrish, D.; Yager, K.; Saunders, M.; Shenderovich, M.; Roth, B.L.; McKinnon, R.; et al. Lead optimization of purine based orally bioavailable Mps1 (TTK) inhibitors. *Bioorg. Med. Chem. Lett.* **2012**, *22*, 4377–4385. [CrossRef] [PubMed]
24. Janíková, K.; Jedinák, L.; Volná, T.; Cankař, P. Chan-Lam cross-coupling reaction based on the Cu_2S/TMEDA system. *Tetrahedron* **2018**, *74*, 606–617. [CrossRef]
25. Jedinák, L.; Zátopková, R.; Zemánková, H.; Šustková, A.; Cankař, P. The Suzuki-Miyaura Cross-Coupling Reaction of Halogenated Aminopyrazoles: Method Development, Scope, and Mechanism of Dehalogenation Side Reaction. *J. Org. Chem.* **2017**, *82*, 157–169. [CrossRef]
26. Magano, J.; Dunetz, J.R. Large-scale applications of transition metal-catalyzed couplings for the synthesis of pharmaceuticals. *Chem. Rev.* **2011**, *111*, 2177–2250. [CrossRef]
27. Tomanová, M.; Jedinák, L.; Košař, J.; Kvapil, L.; Hradil, P.; Cankař, P. Synthesis of 4-substituted pyrazole-3,5-diamines via Suzuki-Miyaura coupling and iron-catalyzed reduction. *Org. Biomol. Chem.* **2017**, *15*, 10200–10211. [CrossRef]
28. Hendrychova, D.; Jorda, R.; Kryštof, V. How selective are clinical CDK4/6 inhibitors? *Med. Res. Rev.* **2021**, *41*, 1578–1598. [CrossRef]
29. Gucky, T.; Reznickova, E.; Radosova, M.T.; Jorda, R.; Klejova, Z.; Malinkova, V.; Berka, K.; Bazgier, V.; Ajani, H.; Lepsik, M.; et al. Discovery of N(2)-(4-Amino-cyclohexyl)-9-cyclopentyl- N(6)-(4-morpholin-4-ylmethyl-phenyl)- 9H-purine-2,6-diamine as a Potent FLT3 Kinase Inhibitor for Acute Myeloid Leukemia with FLT3 Mutations. *J. Med. Chem.* **2018**, *61*, 3855–3869. [CrossRef]
30. Chen, P.; Lee, N.V.; Hu, W.; Xu, M.; Ferre, R.A.; Lam, H.; Bergqvist, S.; Solowiej, J.; Diehl, W.; He, Y.A.; et al. Spectrum and degree of CDK drug interactions predicts clinical performance. *Mol. Cancer Ther.* **2016**, *15*, 2273–2281. [CrossRef]
31. Li, Z.; Wang, X.; Eksterowicz, J.; Gribble, M.W., Jr.; Alba, G.Q.; Ayres, M.; Carlson, T.J.; Chen, A.; Chen, X.; Cho, R.; et al. Discovery of AMG 925, a FLT3 and CDK4 dual kinase inhibitor with preferential affinity for the activated state of FLT3. *J. Med. Chem.* **2014**, *57*, 3430–3449. [CrossRef]
32. Goldberg, F.W.; Finlay, M.R.V.; Ting, A.K.T.; Beattie, D.; Lamont, G.M.; Fallan, C.; Wrigley, S.M.; Howard, M.R.; Williamson, B.; Vazquez-Chantada, M.; et al. The Discovery of 7-Methyl-2-[(7-methyl[1,2,4]triazolo[1,5-a]pyridin-6-yl)amino]-9-(tetrahydro-2H-pyran-4-yl)-7,9-dihydro-8H-purin-8-one (AZD7648), a Potent and Selective DNA-Dependent Protein Kinase (DNA-PK) Inhibitor. *J. Med. Chem.* **2020**, *63*, 3461–3471. [CrossRef] [PubMed]
33. Eastwood, P.R.; Rodriguez, J.G.; Castillo, E.G.; Taña, J.B. Heteroaryl Imidazolone Derivatives as Jak Inhibitors. WO2011157397A1, 22 December 2011.

34. Stadtmueller, H.; Engelhardt, H.; Schoop, A.; Steegmaier, M. Pteridinones Used as plk (Polo Like Kinase) Inhibitors. WO2006021547, 2 March 2006.
35. Adachi, K.; Kuroda, Y.; Furuta, T.; Fujii, Y. 2-Amino Substituted 8-Oxodihydropurine Derivative. Patent JP2012184205A, 27 September 2012.
36. Jorda, R.; Hendrychova, D.; Voller, J.; Reznickova, E.; Gucky, T.; Krystof, V. How selective are pharmacological inhibitors of cell-cycle-regulating cyclin-dependent kinases? *J. Med. Chem.* **2018**, *61*, 9105–9120. [CrossRef] [PubMed]
37. Jorda, R.; Havlicek, L.; Perina, M.; Vojackova, V.; Pospisil, T.; Djukic, S.; Skerlova, J.; Gruz, J.; Renesova, N.; Klener, P.; et al. 3,5,7-Substituted Pyrazolo[4,3-d]Pyrimidine Inhibitors of Cyclin-Dependent Kinases and Cyclin K Degraders. *J. Med. Chem.* **2022**, *65*, 8881–8896. [CrossRef] [PubMed]
38. Trott, O.; Olson, A.J. AutoDock Vina: Improving the speed and accuracy of docking with a new scoring function, efficient optimization, and multithreading. *J. Comput. Chem.* **2010**, *31*, 455–461. [CrossRef] [PubMed]
39. Adasme, M.F.; Linnemann, K.L.; Bolz, S.N.; Kaiser, F.; Salentin, S.; Haupt, V.J.; Schroeder, M. PLIP 2021: Expanding the scope of the protein-ligand interaction profiler to DNA and RNA. *Nucleic Acids Res.* **2021**, *49*, W530–W534. [CrossRef] [PubMed]